Seatific

Research Article

The taper ratio influence on the performance of 3-D cavitating hydrofoils moving under a free surface

Şakir BAL*

Department of Naval Architecture and Marine Engineering, İstanbul Technical University, İstanbul, Türkiye

ABSTRACT

This article numerically investigates the taper ratio influence on the performance of three-dimensional (3-D) cavitating hydrofoils moving steadily under a free water surface. The paper modifies and expands upon a previously developed iterative boundary element method (IBEM) to solve this problem. The fluid is assumed to be inviscid and incompressible and to have irrotational flow. All variables and equations have been made non-dimensional to achieve a consistent numerical scheme and very quick convergence. The IBEM iteratively solves the hydrofoil problem and free surface problem separately through the effects they have on each other via their potential values. Both the 3-D hydrofoil surface and the free surface have been modeled using a constant strength source and constant strength doublet panels. The method's results were first validated against those regarding a tapered wing. Later, the model was applied to a tapered hydrofoil to investigate the effects of taper ratio on cavitating hydrofoil performance. The taper ratio has been found to cause a decrease in the drag coefficient on a cavitating hydrofoil, thereby causing an increase in the lift-drag ratio in an unbounded flow domain. The taper ratio also causes a slight improvement in the lift-drag ratio of the cavitating hydrofoil when moving under a free surface.

Cite this article as: Bal Ş. The taper ratio influence on the performance of 3-D cavitating hydrofoils moving under a free surface. Seatific 2023;3:1:1–8.

1. INTRODUCTION

Calculating the hydrodynamic performance of hydrofoils has practical importance, particularly for high-speed foil-assisted racing and sport boats (Pernod et al., 2023). The lift forces these hydrofoils produce can fully or partially support the weight of a marine vessel. However, cavitation can occur on these hydrofoils due to the high-speed flow and small submergence depths hydrofoils have below the free water surface. The taper ratio can also act as a significant geometric parameter on the hydrodynamic performance of these supporting appendages in terms of lift and drag forces and cavitation pattern on the hydrofoil surface. This study numerically investigates the effects of

the taper ratio on cavitating three-dimensional (3-D) hydrofoils moving at constant speed under a free surface using the previously developed iterative boundary element method (IBEM).

Many studies in the past have investigated 3-D hydrofoils moving under (or even piercing) a free water surface with or without cavitation (Bal et al. 2001; Lee & Kerwin, 2003; Bal, 2007; Chen, 2012; Sun & Wu, 2022). Bal et al.'s (2001) study developed an iterative panel method based on Green's theorem to solve the 3-D cavitating hydrofoil problem, applying a low-order panel method with free surface conditions. Lee and Kerwin's (2003) study utilized a high-order panel method based on B-spline fitting for the two-

*Corresponding author.
*E-mail address: sbal@itu.edu.tr

dimensional (2-D) fully submerged hydrofoil problem, but they included no free surface effects in their calculations. Still, the method was very successful at achieving lift forces. Bal (2007) applied a numerical scheme to solve the surface piercing hydrofoil problem that included the cavitation phenomenon in the calculations. That study also considered the effects from angle of attack. Meanwhile, Chen (2012) developed a novel vortex panel method for the potential flow around a 2-D hydrofoil partially submerged under a free water surface using an energy dissipation approach, with dissipative Green functions being employed in the proposed technique. Energy dissipation over a free surface has also been stated to cancel out the singularities of frequency domain integration in the Green functions. Sun and Wu (2022) presented another higher order panel method to solve the inviscid flow around a lifting body. Furthermore, different applications on 2-D bodies moving under free surface can also be found in Uslu and Bal (2008). Pernod et al. (2023) numerically investigated a 2-D submerged hydrofoil moving closely beneath a free water surface using the computational fluid dynamics (CFD) approach. They compared the results from experiments with those from other numerical methods and obtained good satisfaction between the CFD results and the experiments. Celik et al. (2014) also developed a new method for predicting cavity length on two-dimensional and three-dimensional hydrofoils using a potential-based boundary element method. For a given cavitation number, the cavity length on the surface of the two-dimensional hydrofoil was determined by considering the minimum error criterion among different cavity lengths, with the pressure recovery and termination wall models being employed as the cavity termination condition on each section. The agreement the results from this new model had with others was very satisfactory.

Meanwhile, tapered wings are well-known for generating low induced drag, thereby causing an increase in the ratio of the lift-to-drag coefficients (Anderson, 2016; Katz & Plotkin, 2001). Many experimental and numerical studies are found in the past to have occurred on the effects of the taper ratio of wings. This is a very old topic that had interested researchers. For instance, Wetzel (1955) experimentally studied the effects of the taper ratio on the lift, drag, and moment coefficients and showed the taper ratio to have a significant effect on the variation drag coefficient and lift coefficient at a particular Reynolds number. Another experimental analysis in a low-speed wind tunnel was performed to investigate the effects of the taper ratio on the aerodynamic performance of delta wings (Zhang et al., 2009). Their study included an analysis of delta wing models having taper ratios between 0-0.79 and varying with different aspect ratios. Their analysis results showed that wings with taper ratios less than 0.3 have constant lift coefficients, as well as delta wings with a taper ratio between 0.3-0.68 to have increased stall angle and maximum lift as the taper ratio increased. Guzelbey et al.'s (2019) comprehensive study was performed to investigate the effects of the taper ratio of wings on aerodynamic

performance. However, all their studies on the taper ratio effect were done for air wings, not for hydrofoils. They did not consider how very critical the cavitation phenomenon can be for 3-D hydrofoils moving under a free water surface. This current paper modifies the previously developed numerical method (IBEM; Bal & Kinnas, 2002) for cavitating or non-cavitating hydrofoils operating under a free surface and extends it to 3-D hydrofoils with taper ratios. IBEM utilizes Green's theorem (Green's second identity) and defines an integral equation that is based on this theorem. The integral equation is divided into two parts: (i) the hydrofoil part, including its wake and cavity surface, and (ii) the free surface part. These two parts of problem are solved separately. The effects each part has on the other are included iteratively via their potential values. The results from the present IBEM have been validated with experiments and extensively compared with those from other numerical methods for different previous cases (Bal et al., 2001; Bal & Kinnas, 2002, 2003). Another validation study that had not been done before has been added to the paper here. The method is then applied to a 3-D tapered hydrofoil. The effects from the taper ratio have been investigated regarding the lift and drag coefficients, as well as on the cavitation pattern and free surface deformations.

The following sections first summarize the mathematical model of the problem for the completeness of the paper and then introduces a short form for the numerical procedure. Afterward, the sections show the numerical results for a tapered hydrofoil and discuss the effects the taper ratio has on the results with and without cavitation. The paper then concludes with some remarks.

2. MATHEMATICAL MODEL

A cavitating hydrofoil below a free surface is subjected to a uniform inflow U as shown in Figure 1. The x-axis is positive in the direction of uniform inflow, the z-axis is positive upwards, and the y-axis completes the right-handed coordinate system. The origin is located on the intersection point of the mid-span and mid-chord lengths. The undisturbed free surface is located at z = h. The fluid is inviscid and incompressible, and the flow field is irrotational and steady. All variables and equations are non-dimensional. U and c_m are employed for this, where c_m is the mean chord length equal to the average of the c_{root} and c_{tip} values. Figure 1 shows the c_{root} (root chord length) and c_{tip} (tip chord length). The mathematical model has been previously explained in detail (Bal et al., 2001; Bal & Kinnas, 2002) and will explained in brief here for the completeness of the paper.

The perturbation potential $\phi(x, z)$ and the total potential $\Phi(x, z)$ should satisfy Laplace's equation (equation of conservation of mass) in the fluid domain:

$$\nabla^2 \Phi = 0 \text{ and } \nabla^2 \phi = 0 \tag{1}$$

The perturbation potential ϕ should also satisfy the following boundary conditions:
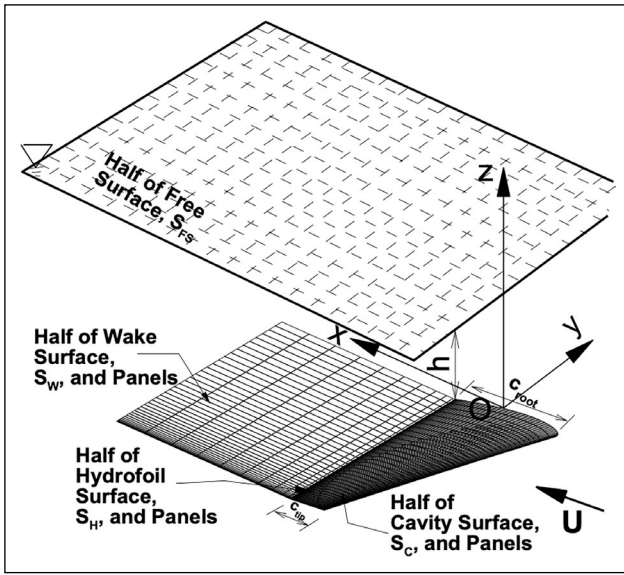
Figure 1. Coordinate system for the 3-D cavitating hydrofoil problem. Only half of the hydrofoil, its wake, and free surface are shown due to the property of symmetry.

1. Kinematic boundary condition on the hydrofoil surface: The total velocity normal to the hydrofoil surface should be zero:

$$\frac{\partial \phi}{\partial n} = -\frac{|\vec{n}|}{c_m} \text{ on } S_H \qquad (2)$$

where $\vec{n}$ is the unit normal vector on the hydrofoil surface and its direction is toward the water. S_H represents the hydrofoil surface.

2. Kutta and wake conditions: The Kutta condition forces a finite velocity at the trailing edge of the hydrofoil along its span-wise direction:

$$\nabla \phi = \text{finite; at the trailing edge} \qquad (3)$$

The force should be zero at the wake surface. The wake surface is assumed to be constant at z=0. The dipole strength at the trailing edge is transferred to the wake surface. thus ensuring the zero pressure jump on the wake surface. Eq. (3) can then be reduced to an iterative Morino's Kutta condition as shown in Kinnas and Hsin (1992) as:

$$\phi^+ - \phi^- = \Delta \phi_w \qquad (4)$$

where ϕ^+ and ϕ^- are the potential values at the respective upper and lower sides of the hydrofoil trailing edge. Details on this condition can be found in Kinnas and Hsin (1992).

3. Dynamic boundary condition on the cavity surface: The pressure should be equal to p_c (vaporize pressure of water) on the cavity surface. Applying Bernoulli's equation, the total velocity q_c can be given as in Kinnas and Fine (1993):

$$q_c/U = \sqrt{1+\sigma} \qquad (5)$$

where σ is the cavitation number defined as:

$$\sigma = \frac{p - p_c}{\frac{1}{2}\rho U^2} \qquad (6)$$

Here, p is the sum of the atmospheric pressure (p_{atm}) and the static pressure ($\rho g h$) far upstream.

4. Cavity closure condition: The cavity is forced to close at its trailing edge (see Kinnas & Fine, 1993). In addition, the cavity detachment point is assumed to be the leading edge of the hydrofoil. This study applies the fixed cavity number solution, which assumes that the cavity number is known and that the cavitation length (cavity volume and cavity planform) must be determined using an iterative technique. Details again can be found in Kinnas and Fine (1993).

5. Linearized free surface condition: If the kinematic and dynamic free surface conditions are combined together and the higher-order terms are neglected, the following linearized free surface equation in non-dimensional form is obtainable as:

$$\frac{\partial^2 \phi}{\partial x^2} + Fr_c^{-2}\frac{\partial \phi}{\partial z} = 0 \text{ on } z=h \qquad (7)$$

Here, Frc is the Froude number $(Fr_c = \frac{U}{\sqrt{gc_m}})$, which is based on the mean chord length, and g is the force of gravity. The corresponding wave elevation in linearized form is also obtainable as:

$$\zeta = -Fr_c^2 \frac{\partial \phi}{\partial x} \qquad (8)$$

Note that ζ is the non-dimensional wave elevation.

6. Radiation condition: Upstream waves should not be on the free surface. This means that the first and second derivatives of the perturbation potential with respect to x are equal to zero for the upstream region on the free surface, which has been demonstrated in Bal and Kinnas (2002) as:

$$\frac{\partial^2 \phi}{\partial x^2} = \frac{\partial \phi}{\partial x} = 0 \text{ as } x \to -\infty \qquad (9)$$

3. THE NUMERICAL APPROACH USING IBEM

According to Green's third identity, the perturbation potential on the hydrofoil surface, its wake, and the free surface can be given as follows:

$$2\pi\phi = \int_{S_H + S_{FS}} \left(\phi \frac{\partial G}{\partial n} - \frac{\partial \phi}{\partial n} G \right) dS + \int_{S_W} \Delta\phi_W \frac{\partial G}{\partial n^+} dS \qquad (10)$$

where S_H, S_W, and S_{FS} are the respective boundaries of the hydrofoil surface, the wake surface, and the free water surface. G is the Green function, and G=1/r, with r being the distance between the singularity point and field point. $\Delta\phi_W$ is the potential jump across the wake surface as given in Eq. (4), and n^+ is the unit vector normal to the wake surface pointing upwards. The present study has modified the iterative method presented mainly in Bal et al. (2001) and applied it to solve Eq. (10). The problem here is divided into two isolated parts: (1) the hydrofoil part, including its wake and cavity surface, and (2) the free surface part. After making some modifications and applying the kinematic boundary condition to the hydrofoil surface and the linearized free surface condition to the z = h plane, Eq. (10) can be divided into two integral equations:

$$2\pi\phi_H = \int_{S_H} \left(\phi \frac{\partial G}{\partial n} + n_x G \right) dS + \int_{S_H} \Delta\phi_W \frac{\partial G}{\partial n^+} dS + 4\pi(\phi_{FS}) \qquad (11)$$

$$2\pi\phi_{FS} = \int_{S_{FS}} \left(\phi \frac{\partial G}{\partial n} + Fr_c^2 \frac{\partial^2 \phi}{\partial x^2} G \right) dS + 4\pi(\phi H) \qquad (12)$$

Here, n_x is the x component of the normal vector on the hydrofoil surface. Integral Equations (11) and (12) can be solved iteratively using a low-order panel method. The potentials ϕ_H and ϕ_{FS} can be updated during the iterative process. The hydrofoil surface and free surface are discretized into small rectangular panels with constant strength source and dipole distributions. The discretized integral equations produce two matrix equations with unknown potentials and can be solved by any matrix solver. The iterative method presented here has two main advantages:

1. Solving for each sub-problem is easier to organize than solving the full problem, and

2. Each sub-problem requires less computational cost (time and memory) than the cost for solving the full problem. Therefore, the total computational time and memory using the iterative process is less than the cost of solving the full problem.

The details for this IBEM can be found in Kinnas and Bal (2002).

4. NUMERICAL RESULTS

The present IBEM has already been validated extensively by comparing the results with experimental data and other numerical methods, as given in Kinnas and Fine (1993) and Bal et al. (2001). Firstly, another validation study has been performed here. The results using the current IBEM have been validated with the experiments for a tapered wing in Cahill and Gottlieb (1950). The tapered wing conforms to the NACA 65A006 airfoil section (Abbott and Doenhoff, 1959). The dihedral angle and twist angle are both zero, while the taper ratio (c_{tip}/c_{root}) is 0.6. Other non-dimensional geometrical parameters are given in Table 1.

The total number of panels used on the hydrofoil surface is 80×80=6,400, with the number of panels in the x and y directions being 80 and 80. The full cosine spacing technique has been applied both in the chordwise and spanwise directions. No free surface effect or cavitation was considered for this particular case. Figure 2 shows the panels used on the full wing with an x-z view of the wing. Figure 3 also shows the lift coefficient and induced drag coefficient ($C_L = \dfrac{L}{\frac{1}{2}\rho AU^2}$ $C_{Dind} = \dfrac{D_{ind}}{\frac{1}{2}\rho AU^2}$; L = lift, D_{ind}= induced drag due to lift, and A = planform area of the wing) in an unbounded flow domain for this study as well as for the experiments taken from Cahill and Gottlieb (1950). A lift coefficient of −0.01 at a 0º angle of attack was measured in the experiments. The possible reason for this may be the very small error introduced while trying to fix the wing's angle of attack in the experiments. Therefore, the lift coefficients have been shifted by an amount of 0.01, which produces a zero-lift coefficient at α = 0° (0º angle of attack), as also suggested in Cetinkaya and Unal (2020). The agreement is very satisfactory up to angle of attack of 8°, beyond which discrepancies occur between the two results (i.e., experiments and IBEM) due to possible flow separation and

Table 1. Geometric details of the wing used in the validation study

Nondimensional span (s)	2
Root (mid-section) chord (c_{root})	0.625
Tip-section chord (c_{tip})	0.375
Sweep Angle	0º
Aspect ratio (AR=s^2/Ar)	4

vortices. The present IBEM has not modeled these physical phenomena. Note also that an α = 12º is the stall angle. The induced drag coefficient due to lift force has also been added to the same figure, with induced drag increasing more than the lift coefficient as angle of attack increases. In addition, the non-dimensional pressure distributions on the mid-strip and tip strip have been demonstrated in Figure 4 at α = 5º. Here, c represents the local chord lengths, namely the mid-strip (section) chord length and tip strip (section) chord length. This shows the loading on the tip section of the hydrofoil to be decreasing as expected.

After this validation, two hydrofoils, namely a rectangular hydrofoil (taper ratio [TR] = c_{tip}/c_{root}=1) and a tapered hydrofoil (TR=3) have been selected to show the effects
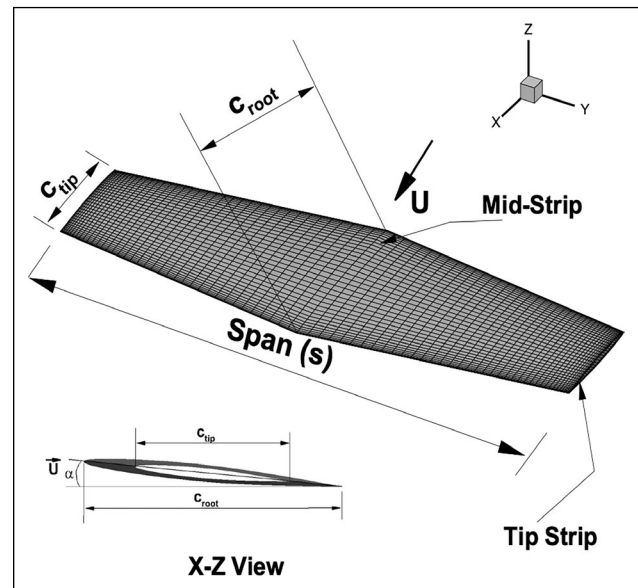
Figure 2. Parameters and panels on the tapered hydrofoil used for validation.
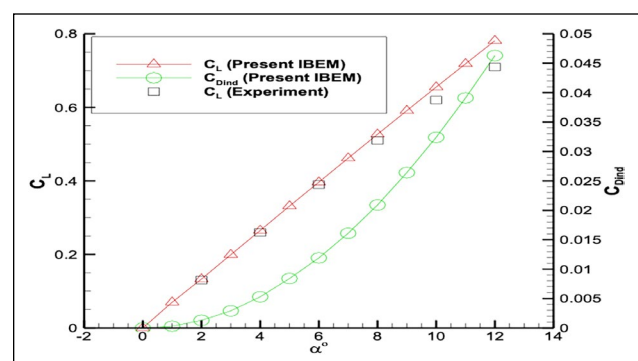
Figure 3. Comparison of lift coefficients with experiments.
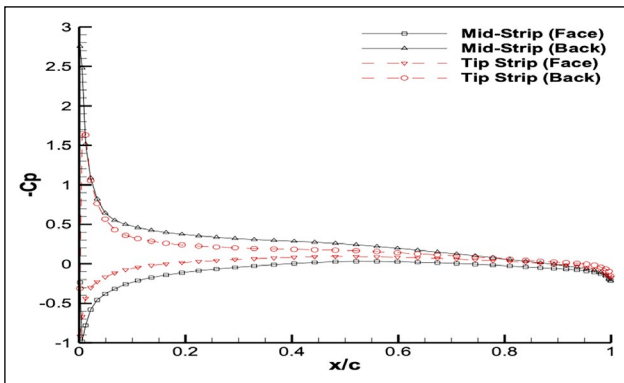
Figure 4. The non-dimensional pressure distribution on mid-section and tip section.
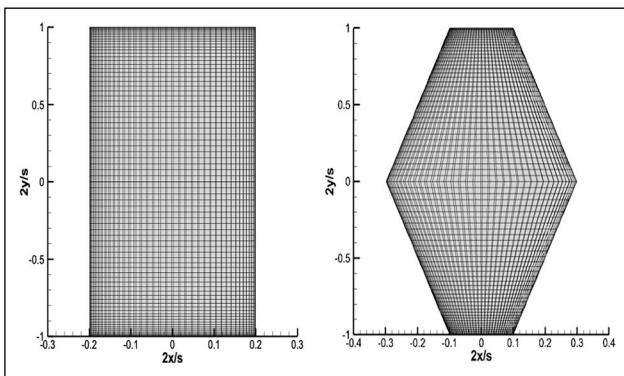
Figure 5. The rectangular (left) and tapered (right) hydrofoils with panels used in the calculations.
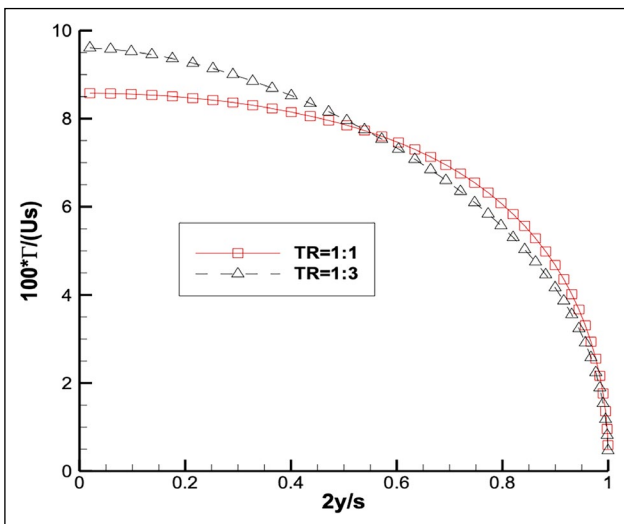
Figure 6. Non-dimensional circulation distribution of rectangular hydrofoil and tapered hydrofoil with no cavitation and no free surface effects. Only half of the distributions are shown due to symmetry.

the taper ratio has on the performance of the hydrofoil in an unbounded flow domain (no free surface effect). Both hydrofoils have the same aspect ratio of 5 (AR=s^2/A; A=planform area of the hydrofoil). The planform areas of both hydrofoils are kept constant. They have no sweep angle and no dihedral angle. Twist angle is also zero. Both

Table 2. Lift and drag coefficients of both hydrofoils in unbounded flow domain

No cavitation	Rectangular (TR=1:1)	Tapered (TR=1:3)
C_L	0.3508	0.3590
$C_{D_{ind}}$	0.0086	0.0087
$C_L/C_{D_{ind}}$	40.9	41.3

Table 3. Lift and drag coefficients of both cavitating hydrofoils in unbounded flow domain

With cavitation, $\sigma=0.7$	Rectangular (TR=1:1)	Tapered (TR=1:3)
C_L	0.3650	0.3634
$C_{D_{ind}}+C_{D_{cay}}$	0.0214	0.0184
$CL/C_{D_{ind}}+C_{D_{cay}}$	17.0	19.8

hydrofoils have the NACA 0012 sections. The angle of attack is fixed and taken as α=5º. The cavitation number is also fixed and equal to σ=0.7. The total number of panels on the hydrofoil surface is 80×80=6,400, with the number of panels in the x direction and y direction being chosen as 80 and 80. The full cosine spacing, both in the chord direction and span direction, have been utilized for all the following simulations. Figure 5 shows both the rectangular hydrofoil and tapered hydrofoil.

First, the non-dimensional circulation distribution along the span direction for both the rectangular and tapered non-cavitating hydrofoils are shown in Figure 6. TR=1:1 and TR=1:3 (TR meaning Taper Ratio) represent the rectangular hydrofoil and tapered hydrofoils, respectively. The loading on the tapered hydrofoil increases more compared to that of the rectangular hydrofoil. This is much clearer in Table 2, which shows the lift and induced drag coefficients for the non-cavitating hydrofoils. Note that the lift coefficient and thereby the ratio of the lift coefficient to the induced drag coefficient increase slightly for the tapered hydrofoil. Next, the lift and the drag (induced+cavity) coefficients for cavitating hydrofoil (σ=0.7) were calculated, with the results given in Table 3. Note that the lift coefficients are almost same, but the ratio of the lift coefficient to the drag (induced+cavity) coefficient has increased for the tapered hydrofoil. This is due to the decrease in the drag (induced+cavity) coefficient. The cavity shapes on both hydrofoils for this particular case are also shown in Figure 7. As can be seen in this figure, the cavitation formation has moved from middle region to the tip region. This is much clearer in Figure 8.

The free surface effects are then included into the calculations. The ratio of submergence depth of the hydrofoil below the free surface to the mean chord length is fixed and equal to h/c_m=1.0. The mean chord length is defined as $c_m=(c_{tip}+c_{root})/2$. The lift coefficients for both the cavitating rectangular and tapered hydrofoils at the
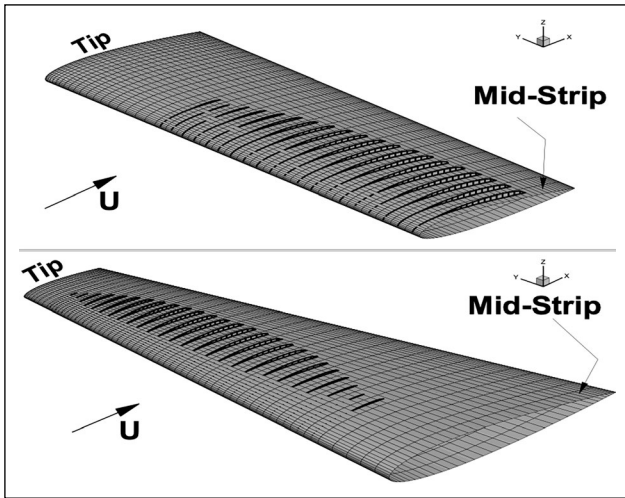
Figure 7. Cavity shapes for rectangular (up) and tapered (down) hydrofoils in unbounded flow domain. Only half of the distributions have shown due to symmetry, α=5º, σ=0.7.
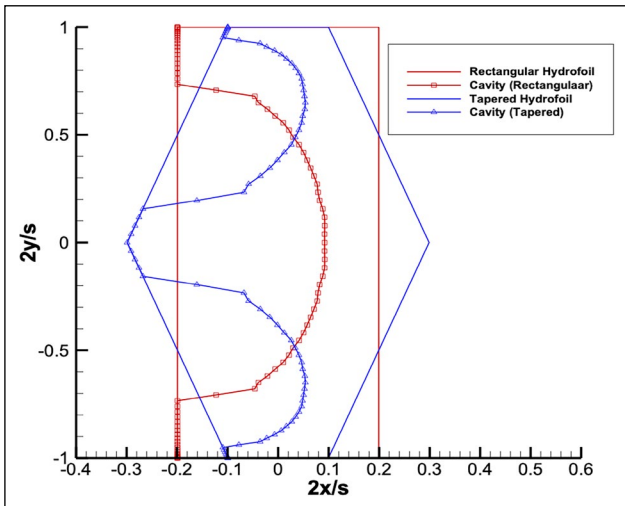
Figure 8. Cavity planforms for rectangular and tapered hydrofoils in unbounded flow domain, α=5º, σ=0.7.

mean chord - based Froude number (Fr$_c$=0.8) are given in Table 4. Free surface causes an increase in lift coefficient as well as in drag coefficient (total drag coefficient is now equal to induced+cavity+wave) compared to those in the unbounded flow domain (Table 3) for this particular case. Meanwhile, the lift-to-drag ratio of the tapered wing is slightly better than that of the rectangular hydrofoil.

The cavity shapes due to the free surface effect on both the rectangular and tapered hydrofoils are shown in Figures 9 and 10, respectively. As can be seen from these figures, the

Table 4. Lift and drag coefficients of both cavitating hydrofoils with free surface effect

With cavitation, σ=0.7, Fr$_c$ = 0.8, h/c$_m$ = 1.0	Rectangular (TR=1:1)	Tapered (TR=1:3)
C$_L$	0.4178	0.4294
C$_{D_{ind}}$+C$_{D_{cay}}$+C$_{D_{way}}$	0.0359	0.0350
CL/(C$_{D_{ind}}$+C$_{D_{cay}}$+C$_{D_{way}}$)	11.6	12.3
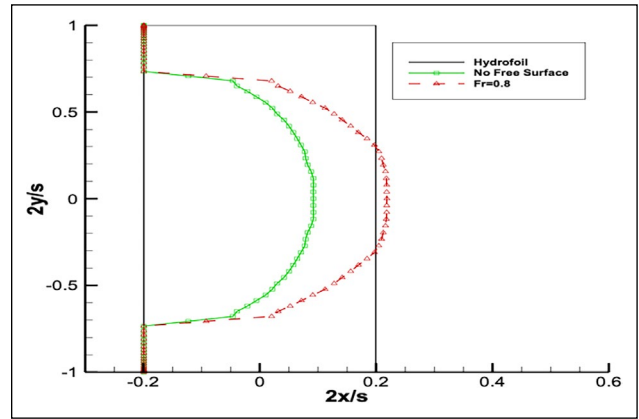
Figure 9. Cavity planforms for rectangular hydrofoil, α=5º, σ=0.7, h/c$_m$=1.0.
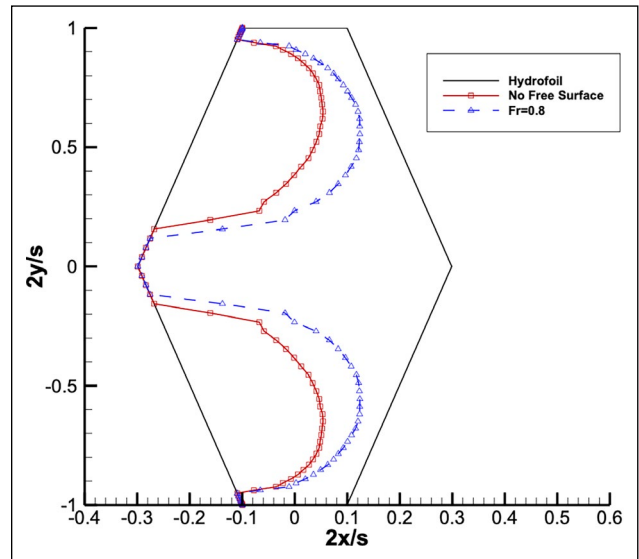
Figure 10. Cavity planforms for tapered hydrofoil, α=5º, σ=0.7, h/c$_m$=1.0.

free surface causes longer cavity lengths for this particular case. Free surface behaves like a solid wall for this particular case, (Bal & Kinnas, 2002).

Figure 11 demonstrates the wave deformations on the free surface for both hydrofoils, showing the Kelvin wave system to have occurred. This can also be seen very clearly in Figure 12, which shows the Kelvin wave contours on the free surface for both the cavitating rectangular and tapered hydrofoils at α=5º, σ=0.7, h/c$_m$=1.0, Fr$_c$=0.8.

4. CONCLUSION

A previously developed iterative numerical method has been made non-dimensional and extended to study the taper ratio effect on 3-D cavitating hydrofoils, with some extensive numerical results being presented. The iterative numerical method was first applied to a tapered rectangular hydrofoil for a validation study, and very good agreement has been found between the results from the present IBEM and those from the experiments. The numerical method was later applied to rectangular and tapered cavitating
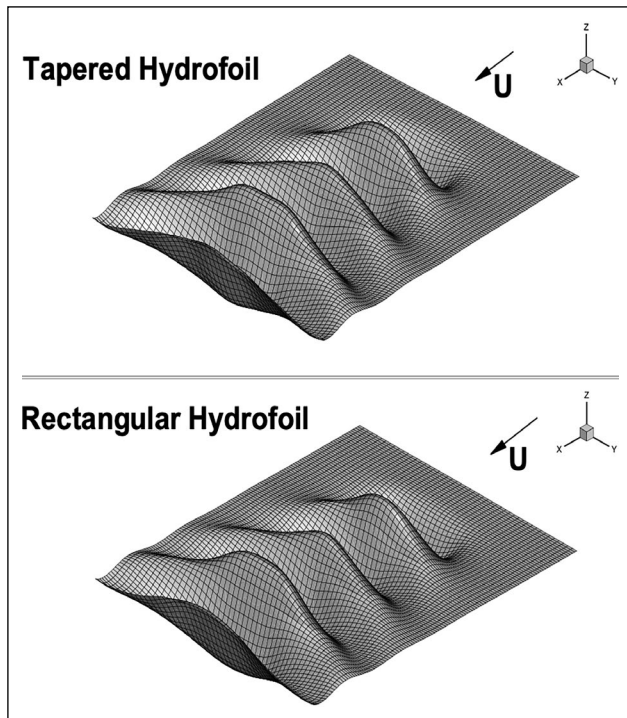
Figure 11. Wave deformation on free surface for both hydrofoils; $\alpha=5^\circ$, $\sigma=0.7$, $h/c_m=1.0$, $Fr_c=0.8$.
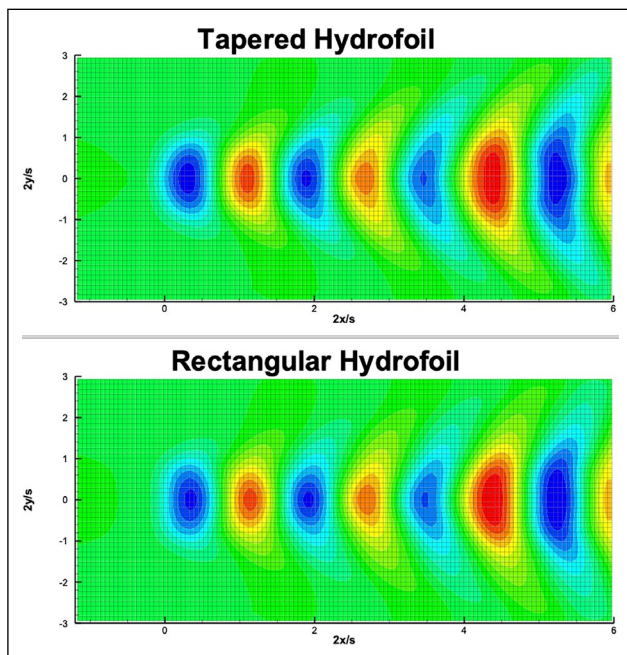
Figure 12. Kelvin wave contours on free surface for both hydrofoils; $\alpha=5^\circ$, $\sigma=0.7$, $h/c_m=1.0$, $Fr_c=0.8$.

hydrofoils to predict hydrodynamic performance, with the following conclusions having been found:

1. Cavitation causes an increase in loading on the hydrofoil due to a virtual camber effect.

2. Cavitation causes an increase in lift coefficient as well as in drag coefficient. But the lift-to-drag ratio decreases drastically due to the increase in drag coefficient being much higher.

3. The taper ratio causes a decrease in the drag coefficient on a cavitating hydrofoil, thereby causing an increase in lift-to-drag ratio.

4. The taper ratio causes a slight improvement to the lift-to-drag ratio for the cavitating hydrofoil moving under a free surface.

NOMENCLATURE

A	: Planform area
AR	: Aspect ratio
c_m	: Mean chord length
c_{tip}	: Chord length at tip
c_{root}	: Chord length at root (mid-section)
C_{Dcav}	: Cavity drag coefficient
C_{Dind}	: Induced drag coefficient due to lift
C_{Dtot}	: Total drag coefficient
CD_{wav}	: Wave drag coefficient
C_L	: Lift coefficient
C_P	: Pressure coefficient
D_{cav}	: Cavity drag
D_{ind}	: Induced drag
D_{tot}	: Total drag
D_{wav}	: Wave drag
Fr	: Chord-based Froude number, Fr :U/(gcm)0.5
g	: Gravitational acceleration
h	: Submerged depth of hydrofoil below free surface
IBEM:	Iterative Boundary Element Method
L	: Lift force
$\overrightarrow{n}$	: Unit normal vector directed from hydrofoil to water
p	: Pressure
p_c	: Cavity pressure
p_o	: Reference pressure
q_c	: Velocity on cavity surface
s	: Span
S_C	: Cavity surface
S_{FS}	: Free surface
S_H	: Hydrofoil surface
S_W	: Wake surface
t_{max}	: Maximum thickness
U	: Velocity of incoming flow
α	: Angle of attack
Φ	: Total potential
ϕ	: Perturbation potential
ρ	: Density of water
σ	: Cavitation number
ζ	: Wave elevation

DATA AVAILABILITY STATEMENT

The published publication includes all graphics and data collected or developed during the study.

CONFLICT OF INTEREST

The author declared no potential conflicts of interest with respect to the research, authorship, and/or publication of this article.

ETHICS

There are no ethical issues with the publication of this manuscript.

FINANCIAL DISCLOSURE

The authors declared that this study has received no financial support.

REFERENCES

Abbott, I. H., & Doenhoff, A. V. (1959). *Theory of wing sections* (1st ed.). Dover Publications.

Anderson, J. (2016). *Fundamentals of aerodynamics* (6th ed.). McGraw-Hill.

Bal, S., Kinnas, S. A., & Lee, H. (2001). Numerical analysis of 2-D and 3-D cavitating hydrofoils under a free surface. *Journal of Ship Research*, *45*(1), 34–49. [CrossRef]

Bal, S., & Kinnas, S. A. (2002). A BEM for the prediction of free surface effect on cavitating hydrofoils. *Computational Mechanics*, *28*, 260–270. [CrossRef]

Bal, S., & Kinnas, S. A. (2003). A numerical wave tank model for cavitating hydrofoils. *Computational Mechanics*, *32*(4-6), 259–268. [CrossRef]

Bal, S. (2007). High-speed submerged and surface piercing cavitating hydrofoils, including tandem case. *Ocean Engineering*, *34*, 1935–1946. [CrossRef]

Cahill, J. F., & Gottlieb, S. M. (1950). *Low-speed aerodynamic characteristics of a series of swept wings having NACA 65A006 airfoil sections* (Report No. NACA RM L9J20). National Aeronautics and Space Administration.

Celik, F., Arikan, Y. O., & Bal, S. (2014). Numerical simulation of two- and three-dimensional partially cavitating hydrofoils. *Ocean Engineering*, *78*, 22–34. [CrossRef]

Cetinkaya, A., & Unal, U. O. (2020). A computational study into the effect of winglets on the performance of fully submerged hydrofoils. *Applied Ocean Research*, *104*, Article 102357. [CrossRef]

Guzelbey, I. H., Eraslan, Y., & Dogru, M. H. (2019). Effects of taper ratio on aircraft wing aerodynamic parameters: A comparative study. *European Mechanical Science*, *3*(1), 18–23. [CrossRef]

Katz, J., & Plotkin, A. (2001). *Low speed aerodynamics: From wing theory to panel methods* (2nd ed.). McGraw-Hill. [CrossRef]

Kinnas, S. A., & Fine, N. E. (1993). A numerical nonlinear analysis of the flow around two- and three-dimensional partially cavitating hydrofoils. *Journal of Fluid Mechanics*, *254*, 151–181. [CrossRef]

Kinnas, S. A., & Hsin, C. Y. (1992). A boundary element method for the analysis of the unsteady flow around extreme propeller geometries. *AIAA Journal*, *30*, 688–696. [CrossRef]

Lee, C. S., & Kerwin, J. E. (2003). A B-spline higher order panel method applied to two-dimensional lifting problem. *Journal of Ship Research*, *47*(4), 290–298. [CrossRef]

Pernod, L., Sacher, M., Wackers, J., Augier, B., & Bot, P. (2023). Free surface effects on two-dimensional hydrofoils by RANS-VOF simulations. *Journal of Sailing Technology*, *8*(1), 24–33. [CrossRef]

Sun, S. Y., & Wu, G. X. (2022). Inviscid flow passing a lifting body with a higher order boundary element method. *Engineering Analysis with Boundary Elements*, *136*, 144–157. [CrossRef]

Uslu, Y., & Bal, S. (2008). Numerical prediction of wave drag of 2-D and 3-D bodies under or on a free surface. *Turkish Journal of Engineering and Environmental Sciences*, *32*, 177–188.

Wetzel, B. E. (1955). Effect of taper ratio on lift, drag, and pitching moment characteristics of thin wings of aspect ratio 3 with 53.1° sweepback of leading edge at subsonic and supersonic speeds. NACA RM A54J20.

Zhang, P. F., Wang, J. J., Liu, Y., & Wu, Z. (2009). Effect of taper ratio on aerodynamic performance of cropped non-slender delta wings. *Journal of Aircraft*, *46*(1), 320–325. [CrossRef]